Computational discovery of a dynamically stable cubic SH_3-like high-temperature superconductor at 100 GPa via CH_4 intercalation

Ying Sun,[1] Yifan Tian,[1] Bowen Jiang,[1] Xue Li,[1] Hefei Li,[1] Toshiaki Iitaka,[2] Xin Zhong,[3,4,*] and Yu Xie[1,†]

[1]*State Key Laboratory for Superhard Materials and International Center for Computational Method & Software and Key Laboratory of Physics and Technology for Advanced Batteries (Ministry of Education), College of Physics, Jilin University, Changchun 130012, China*

[2]*Computational Astrophysics Laboratory, RIKEN, 2-1 Hirosawa, Wako, Saitama 351-0198, Japan*

[3]*Center for High Pressure Science and Technology Advanced Research, Changchun 130012, China*

[4]*Key Laboratory of Functional Materials Physics and Chemistry of the Ministry of Education, Jilin Normal University, Changchun 130103, China*

(Received 15 January 2020; revised manuscript received 13 March 2020; accepted 25 March 2020; published 4 May 2020)

The 203 K superconductivity of SH_3 stimulates enormous interest in searching for high-temperature superconductors in compressed hydrides. While several hydrides show high-temperature superconductivity (>180 K) at extremely high pressure, it is highly desired to design hydrides that can achieve similar superconductivity at relatively lower pressure. In this work we identify a cubic structure in ternary CSH_7 that can be viewed as methane (CH_4) molecules inserted into the SH_3 host lattice as a guest. Ionic bonding in this special host-guest arrangement acts as a chemical precompression for SH_3, leading to a much lower predicted dynamically stable pressure of 100 GPa for CSH_7 than that of SH_3 at 170 GPa. Given the superhigh superconductivity of the parent SH_3 sublattice, we performed electron-phonon coupling calculations to estimate the T_c of CSH_7 at high pressure, which could reach 181 K at 100 GPa. Our results may shed light on the design principle for other multinary host-guest high-temperature superconducting hydrides with low stable pressure.

DOI: 10.1103/PhysRevB.101.174102

I. INTRODUCTION

Seeking of the room-temperature superconductor is one of the most significant challenges in condensed matter physics. As the lightest element, metallic hydrogen should have the highest vibrational frequency and strong electron-phonon interaction. Thus it is the most likely to become a room-temperature superconductor based on BCS theory [1,2]. Although various theoretical calculations predicted metallic hydrogen to show high superconducting temperature T_c ranging from 100 to 760 K [3–5], the metallization of hydrogen has never been fully confirmed by experiments up to 495 GPa [6,7].

Alternatively, metallic hydrides with high hydrogen content were proposed to be another way to approach high-temperature superconductivity at relatively lower pressure [8,9]. In hydrides, interaction between the nonhydrogen atoms and a hydrogen sublattice acts as a chemical precompression (*e.g.*, SiH_4 [9] and LiH_6 [10]) making the hydrogen sublattice metallic at pressures much lower than that of solid hydrogen. To this end, many attempts have been made to search high-temperature superconducting hydrides (HTSH) in the past two decades [11–13]. However, not until 2014, the first HTSH SH_3 was discovered with a T_c of 203 K at 150 GPa [14–16], which further stimulates the research interests. As a result, including CaH_6 [17], YH_6 [18–22], YH_9 [19,20,22], LaH_{10} [19,20,23,24], $CaYH_{12}$ [25,26], Li_2MgH_{16} [27], and other hydrides [11–13], a number of HTSH have been identified, where LaH_{10} shows the highest T_c ever measured of 250–260 K at 170–180 GPa [19,20,23,24]. In addition, advanced materials informatics and machine learning approaches have also been used to predict novel HTSH, and several hydrides with T_c values of about 100 K have been proposed ($KScH_{12}$, $GaAsH_6$, RbH_{12}, and CsH_7 showing T_c of 122, 98, 115, and 90 K, respectively) [28,29].

Out of all the proposed HTSH, SH_3 is very special as it is the only covalent prototype with a T_c higher than 200 K. It crystallizes in a cubic structure (space group: 229, $Im\bar{3}m$), where two body-centered cubic [SH_3] sublattices interpenetrate with each other [16]. This covalent three-dimensional (3D) network of H only appears in SH_3 [15,16] and SeH_3 [30,31] for binary hydrides. Due to its uniqueness, many efforts have been devoted to optimizing the superconducting performance of SH_3 by substitution or doping [32–43]. For instance, 2.5% of P ($S_{0.975}P_{0.025}H_3$) can push the T_c to 280 K at 250 GPa [33]. On another hand, Se substitution [37,39] or replacing partial SH_6 octahedron with Xe atoms [36] not only lowers the T_c but also increases the superconducting pressure. While SH_3 and some of its derivatives are indeed high-temperature superconductors, the high superconducting pressure is the main obstacle for the practical application of these HTSH. It is an urgent need to design HTSH with similar T_c but much lower superconducting pressure.

Recently, Snider *et al.* experimentally observed an insulator-metal transition in C-S-H compounds at above

*zhongxin@calypso.cn
†xieyu@jlu.edu.cn

55 GPa, and discussed these compounds as potential superconductors with high transition temperatures at the APS March Meeting in 2019 [44]. Notably, the detailed composition and structure of C-S-H compounds are not determined. Therefore, investigation of the C-S-H system's structural evolution is necessary to provide useful complementary information to experimental observation. Here the high-pressure ternary phase diagram of the C-S-H system at 100 GPa is constructed through extensive structural searches via the swarm intelligence-based CALYPSO method [45–47]. In particular, a unique host-guest CSH_7 compound has been predicted, where C and H form methane molecules CH_4 and insert them into the $[SH_3]$ sublattice. Importantly, CSH_7 is dynamical stable at pressures as low as 100 GPa. Analysis suggests this might originate from the precompression as the ionic interaction between CH_4 and $[SH_3]$ sublattice is enhanced when pressure increases. Subsequent electron-phonon coupling calculations indicate this phase is likely to be a high-temperature superconductor with a T_c of 181 K at 100 GPa. Our results indicate that the interaction in the host-guest hydride CSH_7 greatly reduces the stable pressure of the $[SH_3]$ host lattice, which may act as useful guidance to lower the stable pressure of more high-temperature superconducting hydrides.

II. COMPUTATIONAL DETAILS

Universal variable-composition structure searches for $C_xS_yH_z$ ($x = 1 - 4$, $y = 1 - 4$, $z = 1 - 36$) were performed at 100 GPa with the CALYPSO structure prediction method [45–47], which requires only chemical compositions for given compounds to predict stable or metastable structures at a given pressure, using simulation cells that consist of a maximal number of 50 atoms. To ensure the highest prediction efficiency, the particle swarm optimization (PSO) technology combined with the symmetry constraints on structural generation was used to generate the child structures following the current optimal structure. In total, 330 different compositions, where nearly 400 structures for each stoichiometry have been studied. For 87 compositions with a formation enthalpy (compared to the most competing elements, binaries and ternaries) lower than 100 meV/atom, further fixed-composition structural predictions were conducted until they reached the convergence after we generated 3000 structures per stoichiometry.

The underlying structural relaxation was carried out within the framework of density functional theory as implemented in the Vienna *ab initio* simulation package (VASP) [48]. The electron-ion interaction was described by projector-augmented-wave (PAW) potentials [49] with the $2s^22p^2$, $3s^23p^4$, and $1s^1$ configurations treated as valence electrons for C, S, and H, respectively. The generalized gradient approximation (GGA) [50] in the scheme of Perdew-Burke-Ernzerhof (PBE) [51] was chosen for the exchange-correlation functional, and kinetic cutoff energy of 800 eV and Monkhorst-Pack $\boldsymbol{k}$ meshes with grid spacing of 0.20 $Å^{-1}$ were then adopted to ensure a satisfactory degree of convergence was achieved. Iterative relaxation of atomic positions was stopped when the forces generally acting on the atoms were found to be smaller than 0.01 eV/Å. With this criterion, the change in total energy between successive steps was less than 0.01 meV/cell. The electron localization function (ELF) [52] was used to describe and visualize chemical bonds in molecules and solids. Mulliken population charges [53] were calculated using CASTEP code [54].

Phonon calculations were carried out by using the supercell approach [55] as implemented in the PHONOPY [56], which showed a good agreement with those computed using the Quantum-ESPRESSO [57] and the computational settings described below. Lattice-dynamical and superconducting properties were estimated using density functional perturbation theory (DFPT) [58], performed with the Quantum-ESPRESSO code. Ultrasoft pseudopotentials [59] were used with a kinetic energy cutoff of 100 Ry and the charge density is integrated on a Γ-centered $12 \times 12 \times 12$ $\boldsymbol{k}$-point mesh. A Methfessel-Paxton first-order smearing of 0.02 Ry was applied. The first-order potential perturbation and dynamical matrices were calculated using DFPT on an irreducible $3 \times 3 \times 3$ Γ-centered $\boldsymbol{q}$-point mesh.

Electron-phonon couplings (EPC) constant λ, $\omega_{\log}$, and T_c are solved using the ELK code [60]. T_c are estimated using both the standard Allen-Dynes modified McMillan equation [61] and the Migdal-Eliashberg theory [62–64], and the latter approach gives us the superconducting gap as a function of temperature. The highest temperature for which the superconducting gap value is nonzero defines the critical temperature T_c.

III. RESULTS AND DISCUSSION

Based on the results from the variable-composition structure searches, we constructed the ternary phase diagram of C-S-H as presented in Fig. 1(a). With the higher H content, the compound is found to be more stable, but none of the ternary C-S-H compounds are thermodynamically stable, indicating the ternaries tend to decompose into elements and binaries under certain conditions [16,65–68]. In previous high-throughput material discovery studies, the convention for the threshold between semistable (likely to be synthesized) and unstable (unlikely to be synthesized) compounds is 50 meV/atom [69]. The same convention was adopted in this work. Therefore, metastable ternary C-S-H compounds cannot be precluded. Some possible formation routes to C-S-H ternaries are provided in Table S1 [70] as a candidate reference for experimental synthesis.

Analysis shows there are 44 ternaries with formation enthalpy lower than 50 meV/atom (see the structural parameters of these compounds in Table S3). In these compounds, C atoms always form CH_4 molecules with H atoms. Meanwhile, the coordination number of S is varied from 2 to 6, resulting in different S-H sublattices with distinctive structural features. As the coordination number increases, the S-H sublattice evolves from zero-dimensional (0D) SH_2 molecules, to one-dimensional (1D) S-H chains, then to two-dimensional (2D) S-H planes, and finally become three-dimensional (3D) S-H covalent networks [as shown in Figs. 1(b) and S1]. Except for CH_4 and the S-H sublattice, we also find the existence of H_2-like molecules with a bond length of about 0.75 Å in some C-S-H ternaries.

Previous studies have shown that hydrides containing 3D covalent networks may have relatively high T_c [11–13]. Thus,

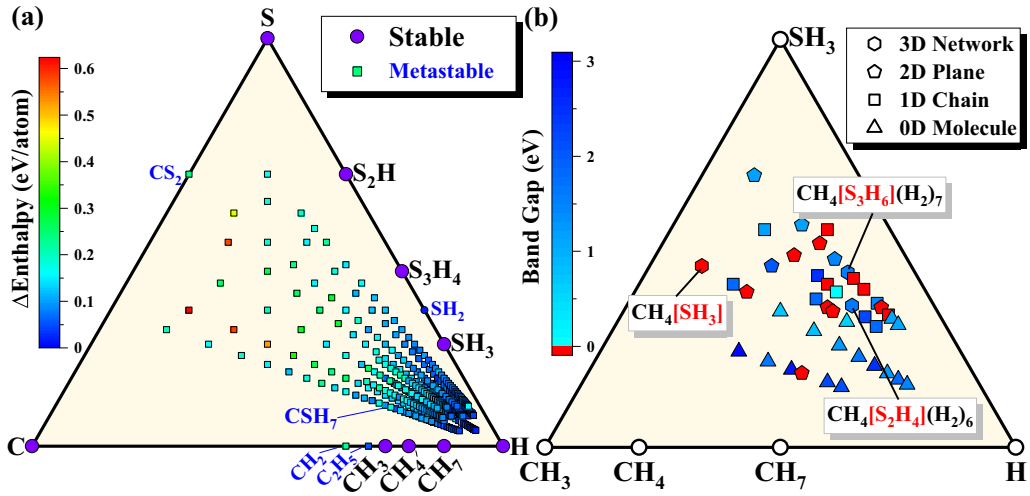

FIG. 1. (a) Calculated stability of the C-S-H system at 100 GPa. Colored squares denote metastable phases with different formation enthalpies. Purple circles indicate stable phases. (b) Bonding behavior and band gap of C-S-H ternary compounds with formation enthalpies below 50 meV/atom at 100 GPa. Colored triangles, squares, pentagons, and hexagons represent different configurations of the S-H sublattice, respectively. Compounds in red or blue are metallic or nonmetallic.

CSH_7, CS_2H_{20}, and CS_3H_{24} with 3D $[SH_3]$, $[S_2H_4]$, and $[S_3H_6]$ covalent networks [Figs. 2(a), S2, and S3] caught our attention. At 100 GPa, CSH_7 crystallizes in a highly symmetrical body-centered cubic structure (space group: $I\bar{4}3m$). CSH_7 only consists of two parts, CH_4 molecules and the $[SH_3]$ sublattice with six-coordinated S, where the latter is identical to the $[SH_3]$ sublattice in $Im\bar{3}m$-SH_3 [15,16] except for the symmetric S-H bonds. Interestingly, each methane molecule

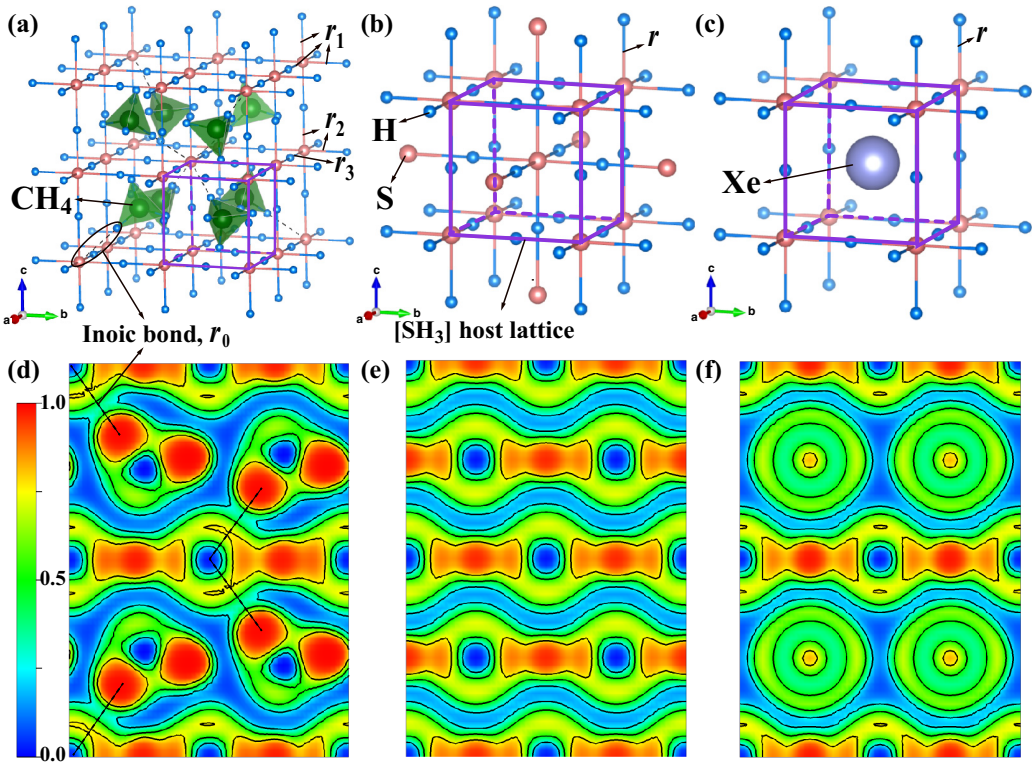

FIG. 2. Conventional cells of (a) $I\bar{4}3m$-CSH_7, (b) $Im\bar{3}m$-SH_3, and (c) $Pm\bar{3}m$-$XeSH_3$. The large, medium, and small spheres represent the Xe, S, and H atoms, respectively, and the translucent regular tetrahedrons represent the CH_4 molecules. Purple lattices represent the $[SH_3]$ host lattice in a unit. (d) ELF in (1 1 0) direction for $I\bar{4}3m$-CSH_7 (left panel) at 100 GPa, $Im\bar{3}m$-SH_3 (middle panel) at 200 GPa, and $Pm\bar{3}m$-$XeSH_3$ (right panel) at 100 GPa. Black dotted lines represent the ionic bonds between the host $[SH_3]$ lattice and the guest CH_4 molecules in $I\bar{4}3m$-CSH_7.

sits in the center of the interstitial space in CSH_7. Therefore, it can be viewed as a host-guest structure. Small charge transfer from $[SH_3]$ host to CH_4 guest was observed as derived from Mulliken population analyses [53] (Fig. S4), which generates negatively charged CH_4 molecules and positively charged $[SH_3]$ framework. An ionic bond between these two oppositely charged ions is represented with the black dotted line in Fig. 2(a). This charge transfer increases with pressure, indicating an enhanced ionic interaction between host and guest sublattices.

Alternatively, S atoms in CS_2H_{20} and CS_3H_{24} form covalent bond with four nearby H atoms, resulting in an $[S_2H_4]$ and $[S_3H_6]$ 3D covalent network, respectively, by sharing H atoms. Besides CH_4, H_2 molecules are also found within the 3D covalent networks. Consequently, in a similar manner to CSH_7, CS_2H_{20} and CS_3H_{24} can be regarded as $CH_4[S_2H_4](H_2)_6$ and $CH_4[S_3H_6](H_2)_7$, respectively. Although the 3D covalent network itself may correspond to high superconductivity, H_2 molecules are not conducive and hydrides with H_2 usually show low superconducting temperature [11,12,17,20,27]. The calculation of the electronic band structure confirms that CS_2H_{20} and CS_3H_{24} with H_2 molecules exhibit nonmetallic characteristics with large band gaps of 1.65 and 1.55 eV at 100 GPa, respectively [as shown in Fig. 1(b)]. We then focus our investigation on CSH_7.

Lattice dynamics simulation shows that CSH_7 and SH_3 will theoretically lose their dynamically stability at pressures of <100 and <170 GPa, respectively (Figs. S5 and S6). As both CSH_7 and SH_3 are mainly consisting of an $[SH_3]$ sublattice, this indicates the intercalation of CH_4 molecules might stabilize an $[SH_3]$ sublattice at a much lower pressure than that of two self-nesting $[SH_3][SH_3]$ sublattices. We have to mention that previous work has also reported on the intercalation of Xe into an $[SH_3]$ sublattice [$Pm\bar{3}m$-$XeSH_3$, Fig. 2(c)] [36]. However, $XeSH_3$ only becomes stable at pressures higher than 240 GPa.

To explore why CSH_7, SH_3, and $XeSH_3$ have the same S-H framework but with different stable pressures, we analyzed the interaction between atoms via the electron localization function (ELF) [52]. At high pressure it is clear that the ELF value between S and H atoms is larger than 0.75 in all three $[SH_3]$ sublattices confirming their covalent nature [Figs. 2(d)–2(f)]. The ELF is around 0.3 between CH_4 and $[SH_3]$ lattice in CSH_7, which is a typical value for ionic bonds [dashed lines in Fig. 2(d)]. In contrast, the ELF is close to 0 between the two sublattices in SH_3 and $XeSH_3$, implying a weak chemical interaction. Analysis of electron charge density [Fig. S7(a)] further confirms the different host-guest interactions among these three compounds as it shows similar behavior to the ELF. Noteworthy, at lower pressure, such as 0 GPa, the ELF turns to be close to 0 between CH_4 and $[SH_3]$ lattice in CSH_7 [Fig. S7(c)], indicating a weakened host-guest interaction. This interaction exists between one of the H atoms of the CH_4 molecule and the apex or body-center S atom of the $[SH_3]$ lattice, that is, the host-guest interaction is anisotropic. Though weakened at lower pressure, chemical interaction between CH_4 and $[SH_3]$ greatly affects the $[SH_3]$ lattice due to its anisotropic character. For instance, H atoms are all symmetrically located between every two S atoms in SH_3 and $XeSH_3$ and the S-H bond length is uniformly distributed. While some H atoms were driven away from their symmetric positions to asymmetric ones in CSH_7 due to the anisotropic interaction, resulting in three different S-H bond lengths (r_1, r_2, and r_3) in Fig. 2(a), especially at 0 GPa (Fig. S8). Upon compression, combined with the pressure-enhancing host-guest ionic interaction, the length of S-H bonds in CSH_7 reduces faster than that in the other two compounds (Fig. S8), thus, the volume of $[SH_3]$ sublattice in CSH_7 also shrinks faster and becomes the smallest one when pressure is higher than 56 GPa (Fig. S9). A smaller volume means a smaller PV term under high pressure which in turn means a lower enthalpy. Thus, the predicted different dynamical stable pressure of CSH_7, SH_3, and $XeSH_3$ might be accounting for the different interaction behaviors, and introducing of the host-guest ionic interactions could be a way to precompress the host hydrides to lower its stable pressure.

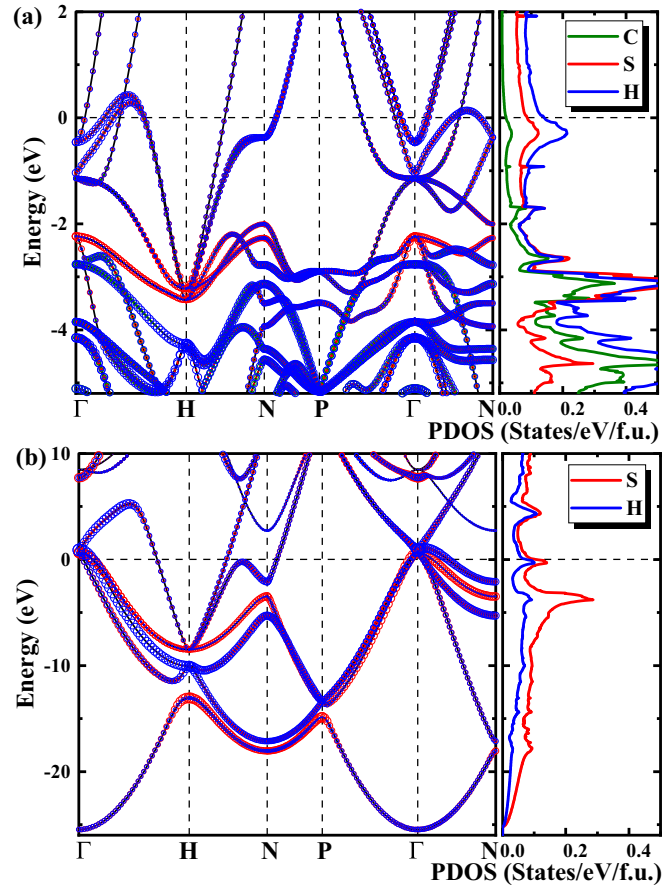

FIG. 3. Electronic band structure (left panel) and projected density of states (right panel) of (a) $I\bar{4}3m$-CSH_7 at 120 GPa and (b) $Im\bar{3}m$-SH_3 at 200 GPa.

Next, we compared the electronic band structures and projected density of states (PDOS) of CSH_7 at 120 GPa with that of SH_3 at 200 GPa (Fig. 3). For CSH_7 (and SH_3) we find for the typical band structural feature near the Fermi level that the band along the $\Gamma \rightarrow N$ direction (and the band near the Γ point) is flat, where the group velocities of the electrons approach zero. In addition, some bands are quite dispersive, such as the band along $H \rightarrow N$ directions for both CSH_7 and SH_3 (Fig. 3). These electronic features apparently satisfy

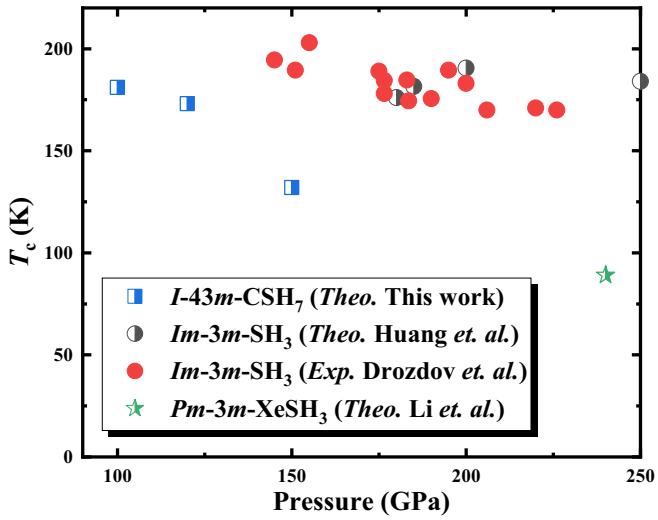

FIG. 4. Pressure dependence of T_c in sulfur hydride. Filled circles show experimental results reported by Drozdov *et al.* [15] while half-filled squares, circles, and stars indicate theoretical results of $I\bar{4}3m$-CSH_7 in this work, $Im\bar{3}m$-SH_3 reported by Huang *et al.* [72], and $Pm\bar{3}m$-$XeSH_3$ reported by Li *et al.* [36], respectively.

the flat band–steep band scenario, which has been suggested to be a favorable condition for the occurrence of superconductivity [71]. Therefore, CSH_7 has a large possibility to be superconductive. Moreover, for the reason that $N(E_F)$ of CSH_7 is comparable to that of SH_3, CSH_7 is expected to be a high-temperature superconductor similar to SH_3.

We further investigated the pressure-dependent superconducting properties of CSH_7, in comparison with SH_3 and $XeSH_3$ (Fig. 4). T_c of SH_3 has been experimentally observed [15] and theoretically calculated [72] to be up to 203 K at 155 GPa and 190 K at 200 GPa, respectively, while the superconducting temperature of $XeSH_3$ was predicted to be just 89 K at 240 GPa [36]. For CSH_7, λ is calculated to be 1.84 at 120 GPa [Fig. S9(a)]. This value is a little bit higher than that of 1.73 for SH_3 at 200 GPa [Fig. S9(c)]. For both CSH_7 and SH_3, H-derived wagging and bending modes (500–1300 cm^{-1}) contribute the most (68% and 83%, respectively) of the total λ, while the S-derived acoustic mode (0–300 cm^{-1}) contribute the rest (32% and 17%, respectively). High-frequency vibrations (3200–3500 cm^{-1}) are not observed in SH_3 due to the absence of the CH_4 molecules. T_c of CSH_7 is evaluated both through the direct numerical solution of the Allen-Dynes modified McMillan equation [61] and the Migdal-Eliashberg equation [62–64], as shown in Table S2. The superconducting gap as a function of temperature at different pressures is given by Fig. S11, where the highest temperature for which the superconducting gap value is nonzero defines the critical temperature T_c. T_c of CSH_7 are then estimated to be 181, 173, and 132 K at 100, 120, and 150 GPa, respectively, using typical Coulomb pseudopotential parameter $\mu^\star = 0.1$ (Figs. 4 and S11). The slightly lowered T_c may correspond to the presence of CH_4 molecules that suppress the electron density of states at the Fermi surface and enhance the Coulomb shielding effect within the crystal lattice.

In addition, the calculation of the electronic band structure identified 13 metal hydrides among the 44 "semistable" compounds. We sampled these hydrides and simulated their superconducting properties. The results showed that C-S-H compounds except for CSH_7 have T_c values less than that of CSH_7 (see Table S1 for more detail) and highlights the unique significance of CSH_7 in C-S-H compounds as a potential high-temperature superconductor. We have to mention that recent studies show phonon anharmonicity can affect the T_c and stable pressure for hydrogen rich materials, especially at high pressures [73–76]. However, these effects will not change the fact that CSH_7 shows similar superconductivity to SH_3 but can be dynamically stable at lower pressures. Thus, anharmonicity was not considered in this work.

IV. CONCLUSION

In summary, we have extensively explored the phase diagram of the C-S-H system at 100 GPa. A unique $I\bar{4}3m$-CSH_7 host-guest hydride with CH_4 guest molecules and [SH_3] host lattice has been identified. CSH_7 is dynamically stable at 100 GPa where the pressure is much lower than that of $Im\bar{3}m$-SH_3 (170 GPa) with similar [SH_3] sublattices. Analysis shows ionic interactions between host and guest lattices may induce chemical precompression and, thus, lower the stable pressure. Calculations suggest CSH_7 is also a high-temperature superconductor with T_c up to 181 K at 100 GPa, where the [SH_3] host lattice mainly contributes to the superconductivity. Our current results show it is possible to reduce the dynamical stable pressure of high superconducting SH_3 with the intercalation of interacting guest molecules, and may also shed light on the high-pressure experimental findings.

ACKNOWLEDGMENTS

This work is supported by the National Natural Science Foundation of China (Grants No. 11534003, No. 11874175, No. 11704151, and No. 11874176), Science Challenge Project No. TZ2016001, National Science Associated Funding (NSAF, Grant No. U1530124), and the Program for Jilin University Science and Technology Innovative Research Team (JLUSTIRT). We used the computing facilities at the High-Performance Computing Centre of Jilin University and Tianhe2-JK at the Beijing Computational Science Research Centre. Part of the calculation was performed in the computing facilities at HOKUSAI system in RIKEN (Japan).

[1] E. Wigner and H. B. Huntington, J. Chem. Phys. **3**, 764 (1935).
[2] N. W. Ashcroft, Phys. Rev. Lett. **21**, 1748 (1968).
[3] L. Zhang, Y. Niu, Q. Li, T. Cui, Y. Wang, Y. Ma, Z. He, and G. Zou, Solid State Commun. **141**, 610 (2007).

[4] P. Cudazzo, G. Profeta, A. Sanna, A. Floris, A. Continenza, S. Massidda, and E. K. U. Gross, Phys. Rev. Lett. **100**, 257001 (2008).

[5] J. M. McMahon and D. M. Ceperley, Phys. Rev. B **84**, 144515 (2011).

[6] P. Dalladay-Simpson, R. T. Howie, and E. Gregoryanz, Nature (London) **529**, 63 (2016).

[7] R. P. Dias and I. F. Silvera, Science **355**, 715 (2017).

[8] C. B. Satterthwaite and I. L. Toepke, Phys. Rev. Lett. **25**, 741 (1970).

[9] N. W. Ashcroft, Phys. Rev. Lett. **92**, 187002 (2004).

[10] E. Zurek, R. Hoffmann, N. W. Ashcroft, A. R. Oganov, and A. O. Lyakhov, Proc. Natl. Acad. Sci. USA **106**, 17640 (2009).

[11] L. Zhang, Y. Wang, J. Lv, and Y. Ma, Nat. Rev. Mater. **2**, 17005 (2017).

[12] H. Wang, X. Li, G. Gao, Y. Li, and Y. Ma, WIREs Comput. Mol. Sci. **8**, e1330 (2018).

[13] J. A. Flores-Livas, L. Boeri, A. Sanna, G. Profeta, R. Arita, and M. Eremets, Phys. Rep. **856**, 1 (2020).

[14] Y. Li, J. Hao, H. Liu, Y. Li, and Y. Ma, J. Chem. Phys. **140**, 174712 (2014).

[15] A. P. Drozdov, M. I. Eremets, I. A. Troyan, V. Ksenofontov, and S. I. Shylin, Nature (London) **525**, 73 (2015).

[16] D. Duan, Y. Liu, F. Tian, D. Li, X. Huang, Z. Zhao, H. Yu, B. Liu, W. Tian, and T. Cui, Sci. Rep. **4**, 6968 (2014).

[17] H. Wang, J. S. Tse, K. Tanaka, T. Iitaka, and Y. Ma, Proc. Natl. Acad. Sci. USA **109**, 6463 (2012).

[18] Y. Li, J. Hao, H. Liu, J. S. Tse, Y. Wang, and Y. Ma, Sci. Rep. **5**, 9948 (2015).

[19] H. Liu, I. I. Naumov, R. Hoffmann, N. W. Ashcroft, and R. J. Hemley, Proc. Natl. Acad. Sci. USA **114**, 6990 (2017).

[20] F. Peng, Y. Sun, C. J. Pickard, R. J. Needs, Q. Wu, and Y. Ma, Phys. Rev. Lett. **119**, 107001 (2017).

[21] I. A. Troyan, D. V. Semenok, A. G. Kvashnin, A. G. Ivanova, V. B. Prakapenka, E. Greenberg, A. G. Gavriliuk, I. S. Lyubutin, V. V. Struzhkin, and A. R. Oganov, https://arxiv.org/abs/1908.01534.

[22] P. P. Kong, V. S. Minkov, M. A. Kuzovnikov, S. P. Besedin, A. P. Drozdov, S. Mozaffari, L. Balicas, F. F. Balakirev, V. B. Prakapenka, E. Greenberg *et al.*, arXiv:1909.10482.

[23] M. Somayazulu, M. Ahart, A. K. Mishra, Z. M. Geballe, M. Baldini, Y. Meng, V. V. Struzhkin, and R. J. Hemley, Phys. Rev. Lett. **122**, 027001 (2019).

[24] A. P. Drozdov, P. P. Kong, V. S. Minkov, S. P. Besedin, M. A. Kuzovnikov, S. Mozaffari, L. Balicas, F. F. Balakirev, D. E. Graf, V. B. Prakapenka *et al.*, Nature (London) **569**, 528 (2019).

[25] X. Liang, A. Bergara, L. Wang, B. Wen, Z. Zhao, X.-F. Zhou, J. He, G. Gao, and Y. Tian, Phys. Rev. B **99**, 100505(R) (2019).

[26] H. Xie, D. Duan, Z. Shao, H. Song, Y. Wang, X. Xiao, D. Li, F. Tian, B. Liu, and T. Cui, J. Phys.: Condens. Matter **31**, 245404 (2019).

[27] Y. Sun, J. Lv, Y. Xie, H. Liu, and Y. Ma, Phys. Rev. Lett. **123**, 097001 (2019).

[28] T. Ishikawa, T. Miyake, and K. Shimizu, Phys. Rev. B **100**, 174506 (2019).

[29] M. J. Hutcheon, A. M. Shipley, and R. J. Needs, arXiv:2001.09852.

[30] S. Zhang, Y. Wang, J. Zhang, H. Liu, X. Zhong, H. F. Song, G. Yang, L. Zhang, and Y. Ma, Sci. Rep. **5**, 15433 (2015).

[31] J. A. Flores-Livas, A. Sanna, and E. K. U. Gross, Eur. Phys. J. B **89**, 63 (2016).

[32] F. Fan, D. A. Papaconstantopoulos, M. J. Mehl, and B. M. Klein, J. Phys. Chem. Solids **99**, 105 (2016).

[33] Y. Ge, F. Zhang, and Y. Yao, Phys. Rev. B **93**, 224513 (2016).

[34] S. Zhang, L. Zhu, H. Liu, and G. Yang, Inorg. Chem. **55**, 11434 (2016).

[35] A. P. Durajski and R. Szczęśniak, Physica C **554**, 38 (2018).

[36] D. Li, Y. Liu, F. Tian, S. Wei, Z. Liu, D. Duan, B. Liu, and T. Cui, Front. Phys. **13**, 137107 (2018).

[37] B. Liu, W. Cui, J. Shi, L. Zhu, J. Chen, S. Lin, R. Su, J. Ma, K. Yang, M. Xu *et al.*, Phys. Rev. B **98**, 174101 (2018).

[38] A. Nakanishi, T. Ishikawa, and K. Shimizu, J. Phys. Soc. Jap. **87**, 124711 (2018).

[39] M. Amsler, Phys. Rev. B **99**, 060102(R) (2019).

[40] J. Chen, W. Cui, J. Shi, M. Xu, J. Hao, A. P. Durajski, and Y. Li, Acs Omega **4**, 14317 (2019).

[41] X. Du, S. Zhang, J. Lin, X. Zhang, A. Bergara, and G. Yang, Phys. Rev. B **100**, 134110 (2019).

[42] K. S. Grishakov, N. N. Degtyarenko, and E. A. Mazur, J. Exp. Theor. Phys. **128**, 105 (2019).

[43] X. Liang, S. Zhao, C. Shao, A. Bergara, H. Liu, L. Wang, R. Sun, Y. Zhang, Y. Gao, Z. Zhao *et al.*, Phys. Rev. B **100**, 184502 (2019).

[44] E. Snider, N. Dasenbrockgammon, and R. Dias, APS March Meeting 2019, cK17.008 (2019).

[45] Y. Wang, J. Lv, L. Zhu, and Y. Ma, Phys. Rev. B **82**, 094116 (2010).

[46] Y. Wang, J. Lv, L. Zhu, and Y. Ma, Comput. Phys. Commun. **183**, 2063 (2012).

[47] B. Gao, P. Gao, S. Lu, J. Lv, Y. Wang, and Y. Ma, Sci. Bull. **64**, 301 (2019).

[48] G. Kresse and J. Furthmüller, Phys. Rev. B **54**, 11169 (1996).

[49] P. E. Blöchl, Phys. Rev. B **50**, 17953 (1994).

[50] J. P. Perdew and Y. Wang, Phys. Rev. B **45**, 13244 (1992).

[51] J. P. Perdew, K. Burke, and M. Ernzerhof, Phys. Rev. Lett. **77**, 3865 (1996).

[52] A. D. Becke and K. E. Edgecombe, J. Chem. Phys. **92**, 5397 (1990).

[53] M. D. Segall, R. Shah, C. J. Pickard, and M. C. Payne, Phys. Rev. B **54**, 16317 (1996).

[54] M. D. Segall, P. J. D. Lindan, M. I. J. Probert, C. J. Pickard, P. J. Hasnip, S. J. Clark, and M. C. Payne, J. Phys.: Condens. Matter **14**, 2717 (2002).

[55] K. Parlinski, Z. Q. Li, and Y. Kawazoe, Phys. Rev. Lett. **78**, 4063 (1997).

[56] A. Togo, F. Oba, and I. Tanaka, Phys. Rev. B **78**, 134106 (2008).

[57] P. Giannozzi, S. Baroni, N. Bonini, M. Calandra, R. Car, C. Cavazzoni, D. Ceresoli, G. L. Chiarotti, M. Cococcioni, I. Dabo *et al.*, J. Phys. Condens. Matter **21**, 395502 (2009).

[58] S. Baroni, S. De Gironcoli, A. Dal Corso, and P. Giannozzi, Rev. Mod. Phys. **73**, 515 (2001).

[59] D. R. Hamann, M. Schlüter, and C. Chiang, Phys. Rev. Lett. **43**, 1494 (1979).

[60] The elk code, http://elk.sourceforge.net/.

[61] P. B. Allen and R. C. Dynes, Phys. Rev. B **12**, 905 (1975).

[62] A. B. Migdal, J. Exptl. Theor. Phys. (U.S.S.R.) **34**, 1438 (1958) [Sov. Phys. JETP **7**, 996 (1958)].

[63] G. M. Eliashberg, J. Exptl. Theor. Phys. (U.S.S.R.) **38**, 966 (1960) [Sov. Phys. JETP **11**, 696 (1960)].
[64] A. Sanna, J. A. Flores-Livas, A. Davydov, G. Profeta, K. Dewhurst, S. Sharma, and E. K. U. Gross, J. Phys. Soc. Jpn. **87**, 041012 (2018).
[65] C. J. Pickard and R. J. Needs, Nat. Phys. **3**, 473 (2007).
[66] H. Liu, I. I. Naumov, and R. J. Hemley, J. Phys. Chem. Lett. **7**, 4218 (2016).
[67] Y. Li, L. Wang, H. Liu, Y. Zhang, J. Hao, C. J. Pickard, J. R. Nelson, R. J. Needs, W. Li, Y. Huang, I. Errea, M. Calandra, F. Mauri, and Y. Ma, Phys. Rev. B **93**, 020103(R) (2016).
[68] N. Zarifi, H. Liu, and J. S. Tse, Sci. Rep. **5**, 10458 (2015).
[69] H. Xiao, Y. Dan, B. Suo, and X. Chen, J. Phys. Chem. C **124**, 2247 (2020).
[70] See Supplemental Material at http://link.aps.org/supplemental/10.1103/PhysRevB.101.174102 for phonon dispersion curves, superconducting properties, and structural parameters of all predicted C-S-H compounds.
[71] A. Simon, Angew. Chem. Int. Edit. **36**, 1788 (1997).
[72] X. Huang, X. Wang, D. Duan, B. Sundqvist, X. Li, Y. Huang, H. Yu, F. Li, Q. Zhou, B. Liu *et al.*, Natl. Sci. Rev. **6**, 713 (2019).
[73] I. Errea, M. Calandra, C. J. Pickard, J. Nelson, R. J. Needs, Y. Li, H. Liu, Y. Zhang, Y. Ma, and F. Mauri, Phys. Rev. Lett. **114**, 157004 (2015).
[74] I. Errea, M. Calandra, C. J. Pickard, J. R. Nelson, R. J. Needs, Y. Li, H. Liu, Y. Zhang, Y. Ma, and F. Mauri, Nature (London) **532**, 81 (2016).
[75] H. Liu, I. I. Naumov, Z. M. Geballe, M. Somayazulu, J. S. Tse, and R. J. Hemley, Phys. Rev. B **98**, 100102(R) (2018).
[76] I. Errea, F. Belli, L. Monacelli, A. Sanna, T. Koretsune, T. Tadano, R. Bianco, M. Calandra, R. Arita, F. Mauri *et al.*, Nature (London) **578**, 66 (2020).